IOPscience iopscience.iop.org

Home Search Collections Journals About Contact us My IOPscience

Transport properties of finite carbon nanotubes under electric and magnetic fields

This article has been downloaded from IOPscience. Please scroll down to see the full text article.

2006 J. Phys.: Condens. Matter 18 10693

(http://iopscience.iop.org/0953-8984/18/47/014)

View the table of contents for this issue, or go to the journal homepage for more

Download details:
IP Address: 129.252.86.83
The article was downloaded on 28/05/2010 at 14:31

Please note that terms and conditions apply.

INSTITUTE OF PHYSICS PUBLISHING JOURNAL OF PHYSICS: CONDENSED MATTER

J. Phys.: Condens. Matter **18** (2006) 10693–10703 doi:10.1088/0953-8984/18/47/014

Transport properties of finite carbon nanotubes under electric and magnetic fields

T S Li[1] **and M F Lin**[2]

[1] Department of Electrical Engineering, Kun Shan University, Taiwan, Republic of China
[2] Department of Physics, National Cheng Kung University, Taiwan, Republic of China

E-mail: mflin@mail.ncku.edu.tw

Received 2 October 2006, in final form 1 November 2006
Published 13 November 2006
Online at stacks.iop.org/JPhysCM/18/10693

Abstract

Electronic and transport properties of finite carbon nanotubes subject to the influences of a transverse electric field and a magnetic field with varying polar angles are studied by the tight-binding model. The external fields will modify the state energies, destroy the state degeneracy, and modulate the energy gap. Both the state energy and the energy gap exhibit rich dependence on the field strength, the magnetic field direction, and the types of carbon nanotubes. The semiconductor–metal transition would be allowed for certain field strengths and magnetic field directions. The variations of state energies with the external fields will also be reflected in the electrical and thermal conductance. The number, the heights, and the positions of the conductance peaks are strongly dependent on the external fields. The heights of the electrical and thermal conductance peaks display a quantized behaviour, while that of the Peltier coefficient does not. Finally, it is found that the validity of the Wiedemann–Franz law depends upon the temperature, the field strength, the electronic structure, and the chemical potential.

1. Introduction

Single-walled carbon nanotubes (SWCNs) are quasi-one-dimensional (Q1D) systems consisting of seamless graphene cylinders with nanometre-size radii [1]. They have been extensively studied because of their unique electronic properties. Only through changing their diameters and chiral angles can carbon nanotubes (CNs) vary from being metallic to semiconducting. By cutting a long CN into segments, a quasi-zero-dimensional finite CN is obtained. The scanning tunnelling microscope has been utilized to produce finite CNs with length of a few tens of nanometres [2]. The reduction in dimensionality leads to many interesting physical phenomena, e.g., quantized standing wave [3]; and novel magnetic [4] and optical properties [5].

 © 2006 IOP Publishing Ltd Printed in the UK

Recently, the electronic transport in mesoscopic systems in whose dimensions are much smaller than the electron mean free path has been extensively studied both experimentally and theoretically [6–10]. One of the most important results is that for an one-dimensional conductor, in the ballistic regime, the electrical conductance is quantized in multiples of the quantum $2e^2/h$, which was first proposed by Landauer [6, 7]. In this system, each current-carrying mode or conducting channel contributes $2e^2/h$ to the electrical conductance. It has been speculated that similar behaviour should exist for the thermal transport. Schwab and collaborators observed the quantum of the thermal conductance, $\kappa_0 = \pi^2 k_B^2 T/3h$, in nanosized narrow wires [11].

Q1D CNs are very suitable systems for studying quantum transport properties. Carrier scatterings will be seriously suppressed in one-dimensional systems because of the limited phase space available. Experimentally, scattering lengths up to several micrometres have been reported in metallic nanotubes [12]. Theoretical calculations show that a conducting SWCN has only two conducting channels, and predict that the electrical conductance will be $4e^2/h$, independent of radius and length [13, 14]. Frank and collaborators found the quantized electrical conductance of multiwalled carbon nanotubes at room temperature [15]. The quantized conductance steps in solutions of multiwalled carbon nanotubes had also been reported by Urbina and co-workers [16]. The experimentally observed linear T dependence of the thermal conductance of SWCNs at low temperature may indicate the existence of quantized thermal conductance in SWCNs [17]. Here, the electrical and thermal transport properties of a finite CN are investigated within the ballistic regime.

2. Tight-binding method

A finite CN is formed by rolling a graphite sheet from the origin to the vector $\mathbf{C_h} = m\mathbf{a_1} + n\mathbf{a_2}$, where $\mathbf{a_1}$ and $\mathbf{a_2}$ are the primitive lattice vectors of the graphene sheet [1]. It has the radius $r = |\mathbf{C_h}|/2\pi = b\sqrt{3(m^2 + mn + n^2)}/2\pi$ and the chiral angle $\xi = \tan^{-1}[-\sqrt{3}\,n/(2m + n)]$. $b = 1.42$ Å is the C–C bond length. The length of the finite CN is determined by the total number of carbon atoms (N_A). Therefore, a finite CN is characterized by $(m, n; N_A)$. With the periodic boundary condition imposed on the electron wavefunction along the circumference, the azimuthal wavevector k_Φ equals J/r, and the angular momentum J is an integer. Details of the geometric and electronic structures of finite CNs are given in [18].

Finite CNs can be classified into three categories according to their energy gaps [18]: (I) moderate-gap semiconductors for energy gaps (E_gs) $\sim$ 1–0.1 eV, (II) narrow-gap semiconductors for E_gs ~ 0.01 eV, and (III) gapless systems for zero E_gs. The main difference between type-II and type-III CNs stems from the curvature effects.

Transport properties of finite CNs under a uniform transverse electric field and a magnetic field with arbitrary polar angle are investigated in this work. We employ the tight-binding model to calculate the electronic structures of CNs. In the presence of a uniform electric field F perpendicular to the nanotube axis, the onsite energy of the ith carbon atom in tight-binding calculations will be perturbed by the amount $\Delta E = -eFr\cos\Phi_i$, with Φ_i being the angle between the field direction and the position of the ith carbon atom along the nanotube circumference. The nanotube axis and the electric field direction are assumed to be the z-axis and x-axis, respectively. The x-axis is chosen in a way that the nanotube is mirror symmetric about it. There is an extra degree of freedom by rotating the nanotube azimuthally; in such a case the nanotube is no longer symmetric about the electric field direction, and a dephasing angle can be defined between the electric field direction and the nanotube symmetric axis. The band structures obtained are almost independent of this dephasing angle except at large field strength, and the effect of the dephasing angle is neglected here.

When a uniform magnetic field passes through a CN, the phase of the electron wavefunction, which is determined by the vector potential, will be modified. The magnetic field is assumed to have the polar angle α. Then the vector potential $\mathbf{A}$ equals $\phi_B \cos\alpha/2\pi r\hat{\Phi} + \phi_B \sin\alpha \sin\Phi/\pi r\hat{z}$, which will induce an extra phase factor $\exp(\mathrm{i}2\pi\Delta G_{\mathbf{R}}/\phi_{B0})$ in the Hamiltonian matrix element between site i and site j. $\Delta G_{\mathbf{R}} = \int_{\mathbf{R}_i}^{\mathbf{R}_j} \mathbf{A}\cdot\mathrm{d}\vec{l}$, $\phi_B = \pi r^2 B$, and $\phi_{B0} = hc/e$ is the magnetic flux quantum.

With the existence of external fields, we need to include all the carbon atoms in the finite CN to construct the nearest-neighbour Hamiltonian, which is an $N_A \times N_A$ Hermitian matrix,

$$H = \sum_i \epsilon_i(\mathbf{F}) c_i^\dagger c_i + \sum_{i,j} t_{i,j}(\mathbf{B}) c_i^\dagger c_j, \tag{1}$$

where $\epsilon_i = -eFr\cos\theta_i$ is the onsite energy and $t_{i,j}$ is the transfer integral between lattice locations i and j; only hopping between the nearest neighbours is considered. $c_i^\dagger$ and c_i are the creation and annihilation operators at site i, respectively. The curvature effect is taken into account by including Kane and Mele's model [19] in assigning the values of $t_{i,j}$s. Their model successfully predicts energy gaps of narrow-gap CNs, which are in excellent agreement with STM measurements [20, 21]. The details of determining $t_{i,j}$s are given in [22].

After diagonalizing the Hamiltonian, the state energy $E^{\mathrm{c,v}}(F,\phi_B,\alpha)$ can be obtained. The superscripts, c and v, represent the conduction bands and the valence bands, respectively. With the inclusion of the Zeeman effect, the total state energy becomes $E^{\mathrm{c,v}}(F,\phi_B,\alpha;\sigma) = E^{\mathrm{c,v}}(F,\phi_B,\alpha) + g\sigma\phi_B/(m^* r^2\phi_{B0})$. The g factor is designated to be the same as that ($\sim$2) of graphite, where $\sigma = \pm 1/2$ is the electron spin and m^* is the bare electron mass.

We consider a finite CN with a transverse electric field and a magnetic field with polar angle α, which is suspended between two reservoirs (macroscopic leads). The left and right reservoirs are assumed to have the chemical potentials and the temperatures $(\mu + eV,\ T)$ and $(\mu,\ T + \Delta T)$, respectively. In the ballistic regime, making use of the Landauer–Buttiker formula, the net electric and thermal currents are, respectively, given by

$$I(F,\phi_B,\alpha) = \frac{e}{h}\int \mathrm{d}E\ T(E,F,\phi_B,\alpha)\left[f^0\left(\frac{E-\mu-eV}{T}\right) - f^0\left(\frac{E-\mu}{T+\Delta T}\right)\right] \tag{2}$$

and

$$U(F,\phi_B,\alpha) = \frac{1}{h}\int \mathrm{d}E\ (E-\mu)T(E,F,\phi_B,\alpha)\left[f^0\left(\frac{E-\mu-eV}{T}\right) - f^0\left(\frac{E-\mu}{T+\Delta T}\right)\right] \tag{3}$$

where f^0 is the Fermi–Dirac distribution function, and the elastic transmission coefficient is approximately given as

$$T(E,F,\phi_B,\alpha) = 2T_{\mathrm{res}}\sum_{E^{\mathrm{c,v}}} \frac{\Gamma^2}{[E^{\mathrm{c,v}}(F,\phi_B,\alpha;\sigma) - E]^2 + \Gamma^2}, \tag{4}$$

where Γ is the broadening width of the electron state energy caused by leaking into the emitter or collector. In this study, Γ is chosen to be $3.3\times10^{-5}\ \gamma_0$ ($\sim$0.1 meV; $\gamma_0 = 3.033$ eV). T_{res} is the transmission probability at resonance ($E^{\mathrm{c}}(F,\phi_B,\alpha;\sigma) = E$).

Within the linear-response approximation ($\Delta T \to 0$ and $V \to 0$), $I(F,\phi_B,\alpha)$ and $U(F,\phi_B,\alpha)$ are reduced to

$$I(F,\phi_B,\alpha) = \mathcal{L}_0(F,\phi_B,\alpha)V - \frac{\mathcal{L}_1(F,\phi_B,\alpha)}{T}\Delta T \tag{5}$$

and

$$U(F,\phi_B,\alpha) = \mathcal{L}_1(F,\phi_B,\alpha)V - \frac{\mathcal{L}_2(F,\phi_B,\alpha)}{T}\Delta T, \tag{6}$$

where

$$\mathcal{L}_\beta(F,\phi_B,\alpha)=\frac{e^{2-\beta}}{h}\int \mathrm{d}E\ (E-\mu)^\beta T(E,F,\phi_B,\alpha)\frac{-\partial f^0(E)}{\partial E}. \tag{7}$$

At low temperatures, the main contributions to $\mathcal{L}_\beta$ ($\beta=1,2,3$) come from electronic states very close to the chemical potential. The electrical conductance is defined by $G=I/V=\mathcal{L}_0$ at $\Delta T=0$. The thermopower, which is the electromotive force (EMF) generated by the system in response to a temperature gradient when $I=0$, is just

$$S=\left.\frac{V}{\Delta T}\right|_{I=0}=\frac{\mathcal{L}_1}{T\mathcal{L}_0}=\frac{\Pi}{T}, \tag{8}$$

where Π is the Peltier coefficient, and this relation between the thermopower and the Peltier coefficient is the well-known Kelvin–Onsager relation. Studying one of the two properties is sufficient. The thermal conductance is defined as the net thermal current produced by a temperature gradient at $I=0$, and is given by

$$\kappa=\left.\frac{-U}{\Delta T}\right|_{I=0}=\frac{\mathcal{L}_2-\mathcal{L}_1^2\mathcal{L}_0^{-1}}{T}. \tag{9}$$

Equation (8) is employed to calculate the Peltier coefficient and equation (9) for the thermal conductance.

3. Results and discussion

We have chosen the type-I (10, 10; 180) CN as a model study. The variations of state energies with the electric field strength F at $\phi_B=0$ are shown in figure 1(a). Electronic energies are symmetric about the Fermi level $E_\mathrm{F}=0$. They touch the Fermi level at certain Fs (0.2, 0.238, 0.374 and 0.382 V Å^{-1}), and vary linearly around these values. The parallel magnetic field ($\alpha=0°$) changes the linear F dependence into a parabolic dependence (figure 1(b)), but not the transverse magnetic field ($\alpha=90°$; figure 1(c)). That the parallel magnetic field would induce a shift in k_Φ from J/r to $(J+\cos\alpha\,\phi_B/\phi_{B0})/r$ is the main reason. The parallel magnetic field also opens an energy gap at $F=0.2$ V Å^{-1}. The Zeeman splitting would introduce a further split for the spin-up and spin-down states. The changes in state energies at $\alpha=90°$ are mainly due to the Zeeman effect (figure 1(c)). The type-I (10, 10; 180) CN is a moderate-gap semiconductor signified by an energy gap $\sim 0.36\gamma_0$ at zero external field. The energy gap is reduced by the transverse electric field, the parallel magnetic field, or the superimposed electric and magnetic fields.

The complex relation between energy gap and external fields deserves a closer examination. The dependence of E_g on the electric field strength F and the magnetic field direction α is shown in figure 1(d). For F less than 0.18 V Å^{-1}, the energy gap decreases with increasing α (figure 1(d)). That is to say, E_g is comparatively easier to be modulated by the transverse magnetic field. For F greater than 0.18 V Å^{-1}, the energy gap displays complicated behaviour with varying F and α. The semiconductor–metal transition takes place for all αs, and the F values leading to the occurrence of such transition depend on α.

The electrical conductance exhibits sharp peak structures with varying F at $T=2$ K, as shown in figure 2. Explanations of the spike behaviour are as follows. The $\partial f(E)/\partial E$ function is a prominent Lorentzian function at the Fermi energy at low temperature. When the lowest states are far from the Fermi level (signified by a nonzero energy gap), G is vanishing. At particular values of F, the lowest states may touch the Fermi level and contribute to the electrical conductance. The positions of the peak correspond to the F values that lead to the

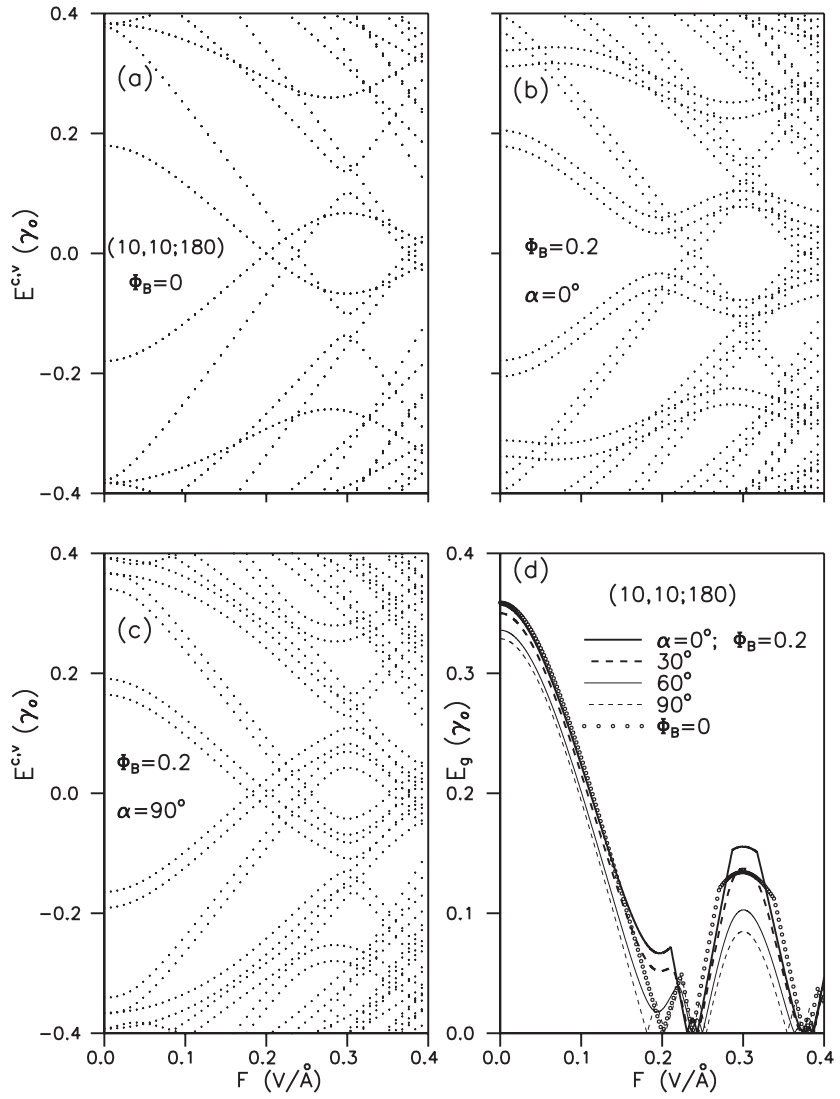

Figure 1. The state energies versus the transverse electric field strength F for a (10, 10; 180) CN at (a) $\phi_B = 0$, (b) $\phi_B = 0.2\phi_{B0}$ and $\alpha = 0°$; (c) $\phi_B = 0.2\phi_{B0}$ and $\alpha = 90°$. (d) Energy gap dependence on F for a (10, 10; 180) CN at $\phi_B = 0$, and $\phi_B = 0.2\phi_{B0}$ with different αs.

semiconductor–metal transitions, and their heights are related to the number of states at the Fermi level. At $\phi_B = 0$, there are four peaks. The inclusion of a magnetic field will change the number, positions and heights of the sharp peaks. The heights of the peaks display quantized behaviour. At $\phi_B = 0$, they are about two times those at $\phi_B = 0.2$ regardless of the value of α. The reason is as follow. At $\phi_B = 0$, the spin-up and spin-down state energies are degenerate, touching the Fermi level at the same F values, and they contribute equally to the electrical conductance. A nonzero ϕ_B will shift the state energies and break the spin degeneracy. The resulting states might or might not cross the Fermi level. If they do cross the Fermi level, the original single peak will separate into two peaks with half of the height. The number of peaks is maximum at $\alpha = 90°$.

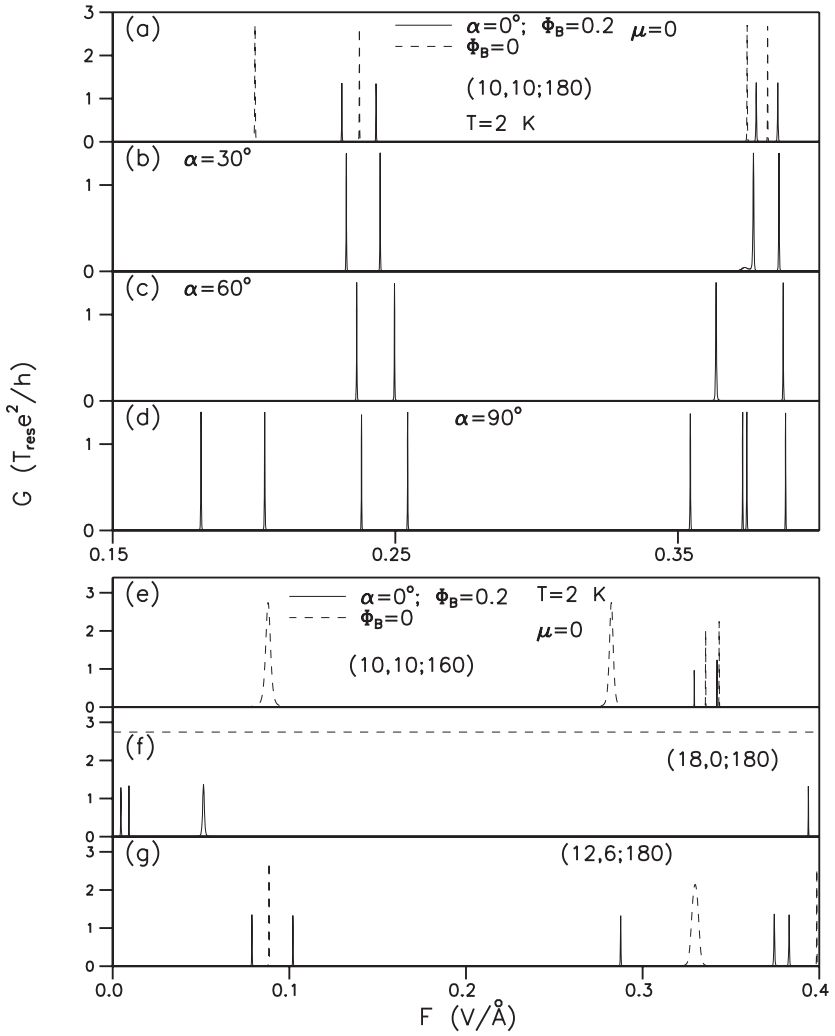

Figure 2. The electric-field-dependent electrical conductance at $T = 2$ K, $\mu = 0$, and $\phi_B = 0.2\phi_{B0}$ for the (10, 10; 180) CN at (a) $\alpha = 0°$, (b) $\alpha = 30°$, (c) $\alpha = 60°$, and (d) $\alpha = 90°$. Electrical conductance dependence on the electric field strength F at $\phi_B = 0.2\phi_{B0}$ and $\alpha = 0°$ for (e) a (10, 10; 160) CN, (f) an (18, 0; 180) CN, and (g) a (12, 6; 180) CN. The cases with $\phi_B = 0$ are shown as dashed line.

We have also calculated the electrical conductance of some other finite CNs: a type-II armchair (10, 10; 160) CN, a type-III zigzag (18, 0; 180) CN, and a type-I chiral (12, 6; 180) CN. All three CNs have roughly the same radii as that of a (10, 10; 180) CN. The ballistic transport properties that we discuss here are found to essentially rely on how the states cross the Fermi energy as the external fields vary. The type of nanotube only affects when and where the crossing occurs. The results we obtained for the type-I armchair (10, 10; 180) CN are general and applicable to other types of nanotube, except for the type-III zigzag (18, 0; 180) CN at $\phi_B = 0$, in which the electrical conductance stays at 2.8 $T_{\rm res}e^2/h$ regardless of F. This is due to the fact that at zero magnetic field, there are always two localized edge states [18] (spin-up and spin-down) at the Fermi energy for a zigzag CN. Although the applied electric

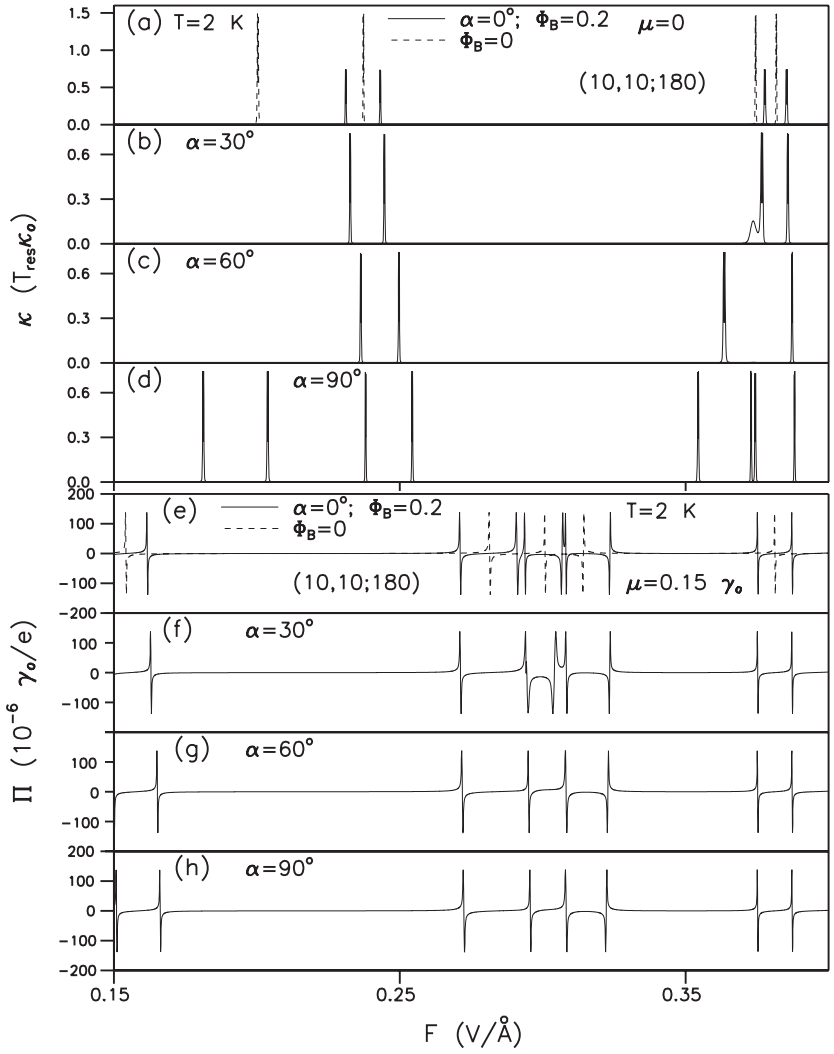

Figure 3. The electric-field-dependent thermal conductance at $T = 2$ K, $\mu = 0$, and $\phi_B = 0.2\phi_{B0}$ for a (10, 10; 180) CN at (a) $\alpha = 0°$, (b) $\alpha = 30°$, (c) $\alpha = 60°$, and (d) $\alpha = 90°$. The electric-field-dependent Peltier coefficient at $T = 2$ K, $\mu = 0.15\gamma_0$, and $\phi_B = 0.2\phi_{B0}$ for a (10, 10; 180) CN at (e) $\alpha = 0°$, (f) $\alpha = 30°$, (g) $\alpha = 60°$, and (h) $\alpha = 90°$. The cases with $\phi_B = 0$ are shown as dashed line.

field modifies the electronic structure, it does not change the number of edge states at the Fermi energy, which is the only factor that determines the conductance.

The number, the heights, and the positions of the thermal conductance peaks are closely corresponding to those of the electrical conductance (figures 3(a)–(d)). The special relationship $\kappa \approx (\pi^2 k_B^2 T/3e^2)G$, as discussed later in equation (12), is the main reason. The differences in the shape and extent of the spikes between the electrical conductance and the thermal conductance originate from the different integrands in equation (7). The integrand of $\mathcal{L}_1$ (equation (7)) is an antisymmetric function of $E - \mu$. When $\mu = 0$, the Peltier coefficient will be identically zero. The computed Peltier coefficient at $\mu = 0.15\gamma_0$ is shown in

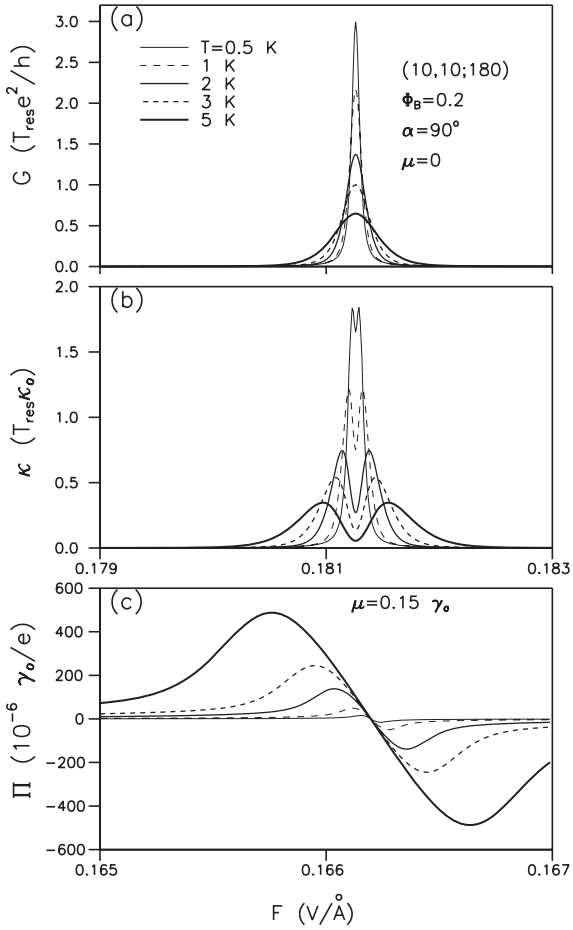

Figure 4. The dependence of (a) the electrical conductance, (b) the thermal conductance, and (c) the Peltier coefficient on the electric field strength F at $\phi_B = 0.2\phi_{B0}$ and $\alpha = 90°$ for a (10, 10; 180) CN at various temperatures.

figures 3(e)–(h). It exhibits an antisymmetric structure, a peak followed by a dip, at resonance. There is a sudden sign change as F varies slightly, which is caused by the antisymmetric nature of $\mathcal{L}_1$. Π becomes weakly dependent on α for large α ($>60°$). Furthermore, the heights of Π do not exhibit quantized behaviour, and they are independent of the spin degeneracy. The functions $\mathcal{L}_0$ and $\mathcal{L}_1$ are individually proportional to the number of degenerate states at the chemical potential, but the ratio or Π is not. Hence the state degeneracy cannot be determined by experimental measurements of Π.

The broadening effects due to temperature are shown in figures 4(a)–(c). The finite temperature smears out the $\partial f(E)/\partial E$ delta function with a width $k_B T$, and consequently changes the number of conducting states. The prominent peak structure of the electrical conductance and the double-peak structure of the thermal conductance are gradually broadened by the increasing temperature. At the same temperature, the integrand of $\mathcal{L}_2$ (equation (7)), which is quadratic in $E - \mu$, is more spread in energy than that of $\mathcal{L}_0$. Therefore, κ is more susceptible to the thermal broadening effect than G. The amplitude of Π grows with temperature, whereas those of G and κ decline.

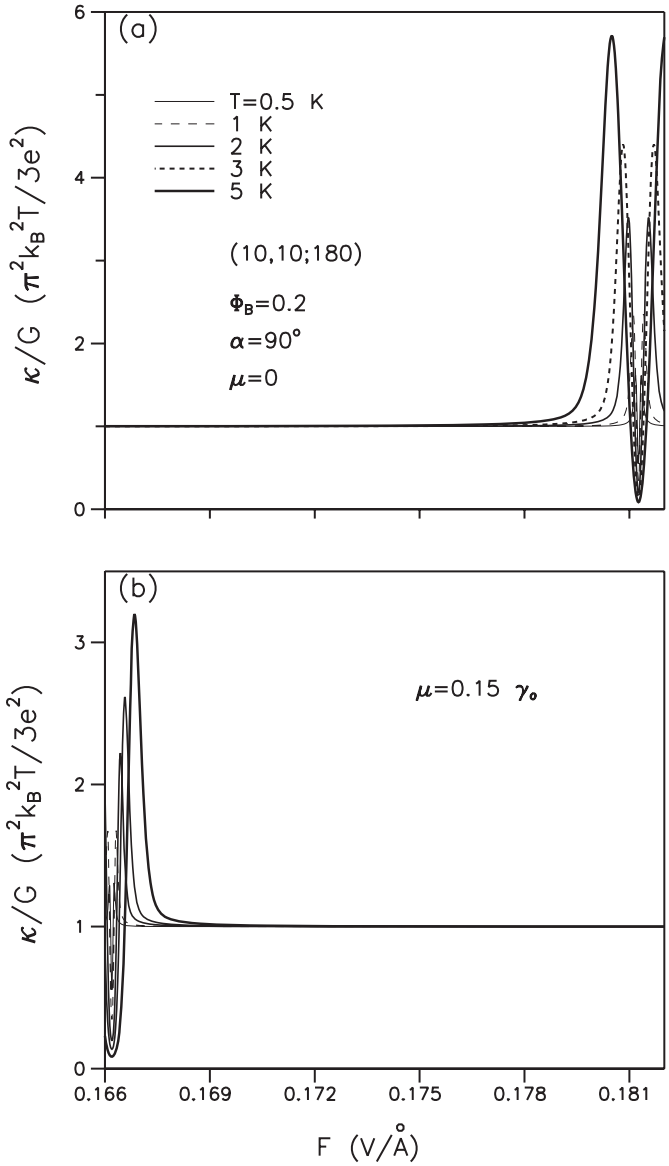

Figure 5. Relation between the thermal conductance and the electrical conductance versus F for a (10, 10; 180) CN at $\phi_B = 0.2\phi_{B0}$ and $\alpha = 90°$ at $\mu =$ (a) 0, (b) 0.15 γ_0 with various temperatures.

At low temperature, making use of the Sommerfeld expansion [23], $\mathcal{L}_2$ can be approximated as

$$\mathcal{L}_2 \approx \frac{\pi^2 k_B^2 T^2}{3e^2}\mathcal{L}_0. \tag{10}$$

For a Q1D infinite CN, as pointed out by Lin and collaborators [24],

$$\mathcal{L}_2 \gg \mathcal{L}_1^2\mathcal{L}_0^{-1}, \tag{11}$$

thus

$$\kappa \approx \frac{\mathcal{L}_2}{T} \approx \frac{\pi^2 k_B^2 T}{3e^2}\mathcal{L}_0 = \frac{\pi^2 k_B^2 T}{3e^2} G, \tag{12}$$

which is the famous Wiedemann–Franz (WF) law, and they found that the WF law is valid when there is no subband crossing the Fermi level. It is of interest to investigate whether this law holds for quasi-zero-dimensional finite CNs. Due to the different temperature dependence, the ratio κ/G fluctuates strongly about 1 (in units of $\pi^2 k_B^2 T/3e^2$) when states approach the chemical potential (figures 5(a) and (b)). The amplitude of fluctuation increases with temperature. On the other hand, the WF law is well obeyed in a wide range of F when the states are far from the chemical potential. Therefore, the validity of the WF law, apart from its dependence on temperature, the external field strength, and the electronic structure, also relies on the chemical potential.

4. Conclusion remarks

In summary, the tight-binding model has been employed to investigate the electronic and transport properties of finite carbon nanotubes subject to the influences of a transverse electric field and a magnetic field with varying polar angle. The external fields will modify the state energies, destroy the state degeneracy, and modulate the energy gap. The state energy and the energy gap exhibit rich dependence on the field strength, the magnetic field direction, and the types of carbon nanotubes. A semiconductor–metal transition would be allowed for certain field strengths and magnetic field directions. The variations of energy dispersions with the external fields will also be reflected in the electrical and thermal conductance. The number, the heights, and the positions of the conductance peaks are strongly dependent on the external fields. The heights of the electrical and thermal conductance peaks exhibit quantized behaviour, while that of Peltier coefficient does not. Finally, it is found that the validity of the Wiedemann–Franz law relies upon the temperature, the external field strength, the band structure, and the chemical potential.

Acknowledgments

This work was supported in part by the National Science Council of Taiwan, the Republic of China under Grant No. NSC 95-2221-E-168-038.

References

[1] Saito R, Fujita M, Dresselhaus G and Dresselhaus M S 1992 *Appl. Phys. Lett.* **60** 2204
[2] Venema L C, Wildoer J W G, Tuinstra H L J T, Dekker C, Rinzler A G and Smalley R E 1997 *Appl. Phys. Lett.* **71** 2629
[3] Rubio A, Portal D S, Artacho E, Ordejon P and Soler J M 1999 *Phys. Rev. Lett.* **82** 3250
[4] Latil S, Henrard L, Bac C G, Bernier P and Rubio A 2001 *Phys. Rev. Lett.* **86** 3160
[5] Compernolle S, Chibotaru L and Ceulemans A 2003 *J. Chem. Phys.* **119** 2854
[6] Landauer R 1957 *IBM J. Res. Dev.* **1** 223
[7] Landauer R 1970 *Phil. Mag.* **21** 863
[8] van Wees B J, van Houten H, Beenakker C W J, Williamson J G, Kouwenhoven L P, van der Marel D and Foxon C T 1988 *Phys. Rev. Lett.* **60** 848
[9] Skocpol W J, Mankiewwich P M, Howard R E, Jackel L D, Tennant D M and Stone A D 1986 *Phys. Rev. Lett.* **56** 2865
[10] Datta S 1995 *Electronic Transport in Mesoscopic Systems* (Cambridge: Cambridge University Press)
[11] Schwab K, Henriksen E A, Worlock J M and Roukes M L 2000 *Nature* **404** 974

[12] McEuen P L, Bockrath M, Cobden D H, Yoon Y G and Louie S G 1999 *Phys. Rev. Lett.* **83** 5098
[13] Lin M F and Shung K W K 1995 *Phys. Rev.* B **51** 7592
[14] Chico L, Benedict L X, Louie S G and Cohen M L 1996 *Phys. Rev.* B **54** 2600
[15] Frank S, Poncharal P, Wang Z L and de Heer W A 1998 *Science* **280** 1744
[16] Urbina A, Echeverria I and Abellan J 2003 *Phys. Rev. Lett.* **90** 106603
[17] Hone J, Whitney M, Piskoti C and Zettl A 1999 *Phys. Rev.* B **59** R2514
[18] Chen R B, Chang C P, Hwang J S, Chuu D S and Lin M F 2005 *J. Phys. Soc. Japan* **74** 1404
[19] Kane C L and Mele E J 1997 *Phys. Rev. Lett.* **78** 1932
[20] Wildoer J W G, Venema L C, Rinzler A G, Smalley R E and Dekker C 1998 *Nature* **391** 59
[21] Ouyang M, Huang J L, Cheung C L and Lieber C M 2001 *Science* **292** 702
[22] Li T S and Lin M F 2006 *Phys. Rev.* B **73** 075432
[23] Ashcroft N W and Mermin N D 1976 *Solid State Physics* (Philadelphia, PA: Saunders College)
[24] Lin M F, Chuu D S and Shung K W K 1996 *Phys. Rev.* B **53** 11186